Diyala Journal of Engineering Sciences

Journal homepage: https://djes.info/index.php/djes

ISSN: 1999-8716 (Print); 2616-6909 (Online)

Analytical Modeling of Transient Thermal Profiles in Rotary Friction Welding of Similar and Dissimilar Materials: 316L Stainless Steel and A60 Carbon Steel

Benfredj Amal, Raouache Elhadj*, Mechta Ahlam, Laouissi Aissa

Department of Mechanical Engineering, University of Bordj Bou Arreridj, Bordj Bou Arreridj, 34000, Algeria

ARTICLE INFO

Article history:
Received 20/01/2026.
Revised: 22/04/2026,
Accepted: 26/05/2026,
Available online: 15/06/2026.
Keywords:
Heat transfer
Mathematical modeling
Rotary friction welding
Separation of variables

ABSTRACT

Rotary friction welding (RFW) is a solid-state joining process widely used for cylindrical components; however, accurate prediction of transient temperature fields remains challenging due to complex frictional heating, material property mismatch, and convective losses. This study develops an analytical model for transient thermal behavior during RFW of 20 mm diameter rods made of similar (316L/316L) and dissimilar (316L/A60) materials at rotational speeds of 710–2000 rpm. Interfacial heat generation is formulated based on thermal effusivity and partitioned between the contacting materials. The three-dimensional transient heat conduction equation in cylindrical coordinates is solved analytically using separation of variables, yielding a Fourier–Bessel series solution. For computational efficiency, the dominant axisymmetric mode (n = 0) is implemented in MATLAB. The model assumes constant thermophysical properties, semi-infinite geometry, axisymmetric heat generation, and lateral convective heat losses. Results show symmetric temperature distributions for similar materials and pronounced asymmetry for dissimilar joints due to differences in thermal conductivity and diffusivity. The predicted peak interface temperature increases nearly linearly with rotational speed, reaching 780.1 °C at 1000 rpm, with deviations below 5% from experimental data (770–800 °C). The heat-affected zone (T > 500 °C) is also accurately predicted. The proposed model provides a fast, physically consistent, and computationally efficient tool for thermal analysis and optimization of RFW processes.

1. INTRODUCTION

Rotary friction welding (RFW) is a solid-state joining technology that is widely utilized in the aerospace, automotive, and heavy machinery industries because it can create high-strength joints without melting the base materials [1-3]. Understanding heat generation in RFW is based on early thermal modeling work. Dawood et al. [1] used simplified energy balance assumptions to construct an analytical thermal model based on frictional heat generation and plastic deformation at the interface. Their findings demonstrated that temperature rise is highly reliant on axial force and rotational speed; nevertheless, the model's forecast accuracy is limited since it ignores transient interfacial changes and assumes unchanging material properties. Although the study is based on steady or semi-steady assumptions, Maalekian [2] employed analytical heat conduction formulae to characterize temperature evolution in friction welding and showed that frictional heating dominates the thermal field. Sluzalec [3] analyzed thermal effects in friction welding using traditional heat transfer theory, demonstrating localized heat concentration at the contact. However, the formulation does not take into consideration complex boundary conditions or material mismatch.

The focus of more recent research has turned to experimental and numerical methods. Mani et al. [4] modeled thermo-mechanical coupling and microstructural evolution in RFW using finite element analysis (FEA). Although the method is computationally costly and heavily dependent on mesh refinement and constitutive law selection, their simulations successfully predicted temperature fields and plastic zones. Alves et al. [5] used thermocouples to perform experimental thermal measurements in dissimilar RFW joints and reported asymmetric heat distribution and severe thermal gradients; nevertheless, the study's prediction power for untested situations is limited. Despite concentrating on linear friction welding, Wanjara et al. [6] employed numerical and experimental methods to show that interfacial plastic flow controls bonding; nevertheless, because of different kinematics, the results cannot be directly applied to rotating configurations.

* Corresponding author's E-mail: elhadj.raouache@univ-bba.dz
DOI: 10.24237/djes.2026.19203

The intricacy of RFW is further highlighted by microstructural and process-based research. Although no formal thermal model was created, studies on stainless steel pipe joints [7] employed experimental welding trials in conjunction with post-weld mechanical characterization to demonstrate that joint strength is very sensitive to interface temperature history. Similar to this, unsymmetrical rod-to-plate RFW investigations [8] showed significant thermal asymmetry brought on by geometric imbalance, but they were unable to forecast temperatures analytically.

Theoretically, transient heat conduction equations in cylindrical coordinates control axisymmetric heat transfer in RFW [9,10]. However, the majority of actual applications use numerical discretization. Despite the lack of closed-form analytical solutions, earlier research [11–14] demonstrated that thermo-mechanical interaction and interfacial evolution are important factors in influencing the temperature distribution. Furthermore, temperature evolution was successfully replicated in finite element simulations by Yohanes et al. [15] and Devotta et al. [16] with good agreement to experimental data, but at the expense of high computing cost and substantial sensitivity to boundary conditions. Process sensitivity is further shown by parametric and experimental research. Joint quality was shown to be strongly dependent on welding parameters by Dhamothara kannan et al. [17] and Chainarong et al. [18]. Nonlinear interactions between process parameters were found through rod-to-plate testing [19] and response surface modeling investigations [20].Although they are still empirical, optimization and review studies [21, 22] used statistical techniques to improve weld quality. Process stability was improved by machine-based modifications [23, 24], but predictive analytical thermal models are still lacking. Despite these developments, current methods are still disjointed: experimental investigations lack broad predictive capability, numerical models are computationally costly, and analytical models are oversimplified. For both identical and dissimilar cylindrical geometries, none offer a single analytical framework for transient temperature prediction in RFW. In their analysis of rotary friction welding, Wenya Li et al. [25] emphasized the lack of a comprehensive analytical predictive model while highlighting the predominance of frictional heat generation. A thermal model for continuous drive friction welding was proposed by Li and Wang [26], although it was based on oversimplified assumptions. Vairis et al. [27] verified basic variations in heat generating mechanisms by comparing friction welding techniques. Friction coefficient-based and coupling-based modeling techniques are further developments. Jin et al. [28] showed that the evolution of interfacial friction controls joint formation, and Jin et al. [29] created thermo-mechanical simulations that can represent bonding evolution. Although they lacked closed-form analytical solutions, Nan et al. [30] used entropy-based modeling. Furthermore, Li et al. [31] offered mathematical expressions for early-stage heating, whereas Tang et al. [32] demonstrated that friction regime transitions have a major impact on the thermal response. Numerical studies continue to show similar limits. Kuo et al. [33] found that peak temperature had a substantial effect on process parameters, whereas Lakache et al. [34] discovered that microstructural evolution was pressure dependent. Furthermore, although both methods are still computationally demanding, Kessler et al. [35] and Mani et al. [4] used finite element and viscoelastic models, respectively. As a result, a number of research [36, 37] have highlighted the need for more precise and effective prediction models. Mathematical tools such as Fourier–Bessel transforms [9] and Bessel function properties [10] provide a strong theoretical foundation for cylindrical heat conduction problems, yet have not been fully exploited for complete RFW analytical modeling.

This study's originality consists in the construction of a unified analytical Fourier-Bessel series model for transient temperature distribution in rotary friction welding of both comparable and dissimilar cylindrical rods. The suggested model offers a closed-form solution that incorporates convective boundary conditions, thermal-effusivity-based heat partitioning, and interfacial frictional heat generation, in contrast to current numerical or simplified analytical methods. Both symmetric and asymmetric thermal fields can be predicted thanks to the model's ability to account for material mismatch effects. One of the first thorough analytical frameworks for RFW thermal analysis, this work provides a computationally effective and physically transparent alternative for process comprehension and optimization.

2. METHODOLOGY

2.1 Geometry and notation

The system consists of two cylindrical rods of equal radius R=10 (diameter 20 mm) aligned along the axial direction (see Figure 1). The rods are in perfect contact at their flat ends, forming the weld interface at z=0. Standard cylindrical coordinates (ρ,ϕ,z) are used, where:

- ρ is the radial coordinate ($0\leq\rho\leq R$),
- ϕ is the azimuthal angle ($0\leq\phi\leq 2\pi$),
- z is the axial coordinate ($z\leq 0$ for Rod 1 (rotating 316L stainless steel) and $z\geq 0$ for Rod 2 (stationary rod, either 316L stainless steel or A60 carbon steel).

Time is denoted by $\tau\geq 0$.

The rotational Reynolds number, which characterizes the effect of rotation on convective cooling, is defined as

$$Re = \frac{\omega R^2}{v} \quad (1)$$

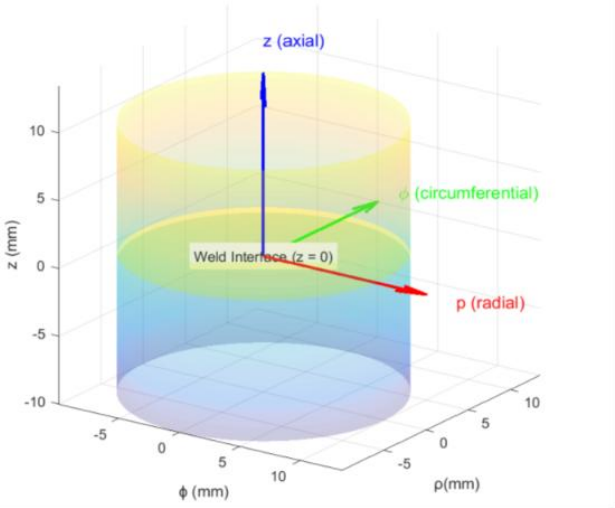

Figure1. Schematic of the rotary friction welding setup

where ω=2πN/60 is the angular velocity (N in rpm), R is the rod radius, and ν is the kinematic viscosity of the surrounding air [6], [9]. The rotational Reynolds number is used to characterize the effect of rotation on convective cooling. In this study, it is introduced as a scaling parameter to represent how increased flow intensity enhances heat dissipation and reduces temperature levels. It is applied in phenomenological manner to capture the influence of operating conditions without being explicitly included in the governing equations.

2.2 Material properties:

The two materials used in this study are 316L austenitic stainless steel and A60 carbon steel. Their chemical compositions and physical/mechanical properties are given in Tables 1 and 2, respectively.

Table 1. Chemical composition of AISI 316L stainless steel and A60 construction steel (determined by X-ray fluorescence spectrometry (XRF))

Material	Cr	C	Mn	Mo	Ni	P	N	Si	Cu	Fe	S
AISI 316L	16.4	0 .04	1.94	2.6	11.65	0.07	0.09	0.68	-	66.53	-
A60	-	-	-	-	-	0.055	0.014	-	-	-	0.055

Table 2. Physical and mechanical properties of A60 structural steel and AISI 316L stainless steel

Material	Melting point (°C)	Thermal conductivity W/m·K	Modulus of elasticity, GPa	Density, kg/m³	Material	Melting point (°C)
316L	1370 – 1400	13 – 16	193	8000	316L	1370 – 1400
A60	1425 – 1540	45 – 60	200	7850	A60	1425 – 1540

2.3 Governing Equations :

The governing equation for heat transfer in cylindrical coordinates is given as follows [6],[9]:

- Rod 1 (z<0):

$$\frac{\partial U_1}{\partial \tau} = \alpha_1 \left[\frac{1}{\rho}\frac{\partial}{\partial \rho}\left(\rho \frac{\partial U_1}{\partial \rho}\right) + \frac{1}{\rho^2}\frac{\partial^2 U_1}{\partial \phi^2} + \frac{\partial^2 U_1}{\partial z^2}\right] \quad (2)$$

- Rod 2(z>0):

$$\frac{\partial U_2}{\partial \tau} = \alpha_2 \left[\frac{1}{\rho}\frac{\partial}{\partial \rho}\left(\rho \frac{\partial U_2}{\partial \rho}\right) + \frac{1}{\rho^2}\frac{\partial^2 U_2}{\partial \phi^2} + \frac{\partial^2 U_2}{\partial z^2}\right] \quad (3)$$

WhereU_1 and U_2 are the transient temperature fields in rod 1 and rod 2, respectively, τ is the time variable,α_1 and α_2 are the thermal diffusivities of rod 1 and rod 2 and ρ, ϕ and z are the radial, circumferential, and axial coordinates, respectively.

2.4 Frictional Heat Generation Model:

Frictional heat at the weld interface (z=0) is the primary source [1], [4]:

$$q(\rho) = \mu P \omega \quad (4)$$

where μ is the friction coefficient is the axial pressure, ω=2πN/60 is the angular velocity, and ρ is the radial coordinate The generated heat is partitioned between the two rods according to the thermal effusivity of each material ei = $\sqrt{k_i \rho_i c_{p,i}}$.

Heat partitioning between the two rods depends on the thermal effusivity of each material [2], [3].

2.5 Boundary and Interface Conditions:

Lateral surface(ρ=R):$-\mathcal{K}_i \frac{\partial U_i}{\partial \rho} = h_i U_i$

Far field (|z|→∞): Ui→0

Interface (z=0): temperature continuity and heat-flux balance with generation.

Initial condition: Ui (ρ,ϕ,z,0)=0

2.6 Separation of variables

Assume [9], [10]:

$$Ui(\rho, \emptyset, z, \tau) = R_1(\rho)\Theta(\phi)Z_1(z)T_1(\tau), 1 = 1,2$$

This assumption reduces the partial differential equations into several ordinary differential equations.

2.6.1Angular solution (common to both rods):

Equation:

$$\frac{d^2\Theta}{d\phi^2} + n^2\Theta = 0, \quad n = 1, 2 \quad (5)$$

Solution:

$$\Theta_n(\phi) = A_n \cos(n\phi) + B_n \sin(n\phi) \quad (6)$$

where n is the azimuthal mode number. For axisymmetric heat generation, the dominant mode is

n=0, An, Bn are constants determined from initial/boundary conditions.

2.6.2 Radial solution (Bessel equation):

Equation:

$$\rho^2 R_i^{''} + \rho R_i^{'} + \left(\lambda_i^2 \rho^2 - n^2\right) R_i = 0 \quad (7)$$

Solution:

$$R_i(\rho) = J_n(\lambda_i \rho), \quad i = 1,2 \quad (8)$$

The eigenvalues λ_{mn} are determined from the convective boundary condition at the lateral surface ρ=R.

$$\lambda_i J_n^{'}(\lambda_i R) + \frac{h_i R}{K_i} J_n(\lambda_i R) = 0 \quad (9)$$

i. *Axial solution (Rod-dependent)*

Equation:

$$\frac{d^2 Z_i}{dz^2} - m_i^2 Z_i = 0 \quad (10)$$

Solution:

$$Z_1(z) = e^{m_1 z}, \quad z < 0 \quad (11)$$

$$Z_2(z) = e^{m_2 z}, \quad z > 0 \quad (12)$$

Where mi is the axial decay parameter for rod i [11]

$$m_i = \sqrt{\frac{2h_i}{K_i R}}, \ i = 1, 2$$

2.6.4 Temporal solution (Rod-dependent):

Equation:

$$\frac{dT_i}{d\tau} + \alpha_i\left(\lambda_i^2 + m_i^2\right) T_i = 0 \quad (13)$$

Solution:

$$T_1(\tau) = e^{-\alpha_1\left(\lambda_1^2 + m_1^2\right)\tau} \quad (14)$$

$$T_2(\tau) = e^{-\alpha_2\left(\lambda_2^2 + m_2^2\right)\tau} \quad (15)$$

$\alpha_i = k_i/\left(\rho_m c_\rho\right)$thermal diffusivity

Interface (weld) conditions at ξ=0

- ✓ Temperature continuity:

$$U_1(\rho, \varphi, 0, \tau) = U_2(\rho, \varphi, 0, \tau)$$

- ✓ Heat flux continuity:

$$k_1 \frac{\partial U_1}{\partial z} = k_2 \frac{\partial U_2}{\partial z}$$

These determine the coefficients C_{np} in the series.

2.6.5Final resolved solution (series form):

Rod 1(z<0):

$$U_1(\rho, \phi, z, \tau) = \sum_{n=0}^{\infty} \sum_{p=1}^{\infty} C_{np} J_n(\lambda_{1P}\rho) \Theta_n(\phi) e^{m_1 z} e^{-\alpha_1\left(\lambda_{1P}^2 + m_1^2\right)} \quad (16)$$

Rod 2(z>0):

$$U_2(\rho, \phi, z, \tau) = \sum_{n=0}^{\infty} \sum_{p=1}^{\infty} C_{np} J_n(\lambda_{2P}\rho) \Theta_n(\phi) e^{m_1} e^{-\alpha_2\left(\lambda_{2P}^2 + m_2^2\right)} \quad (17)$$

The full series coefficients are determined by matching temperature continuity and heat flux balance at the interface z=0.The resulting infinite series solutions were numerically evaluated in MATLAB for practical computation of temperature profiles at different rotational speeds**.**

3.RESULTS AND DISCUSSION

The analytical model, derived from the energy balance and solved using separation of variables, provides the temperature fields $U_1$and U_2as infinite series (equations in Methodology).Numerical simulations in MATLAB approximate these using dominant modes (n=0 for axial/radial, n=1 for circumferential).Profiles are computed at RPM 710, 1000, 1400, and 2000 for 316L (Rod 1) and A60 (Rod 2),We start with similar materials (both rods 316L stainless steel, k=15 W/mK, α=3.75 mm²/s), then transition to dissimilar (Rod 1: 316L, Rod 2: A60 carbon steel, k=50 W/mK, α=13.8 mm²/s).

3.1 Similar Materials Case (Both Rods 316L)

In the similar material case, both rods exhibit identical thermal diffusivity (α = 0.00375 mm²/s) and axial decay parameter (m = 0.5 mm⁻¹), resulting in perfectly symmetric temperature distributions across the weld interface (z = 0).

3.1.1Axial profiles temperature

Figure 2 presents the axial temperature distribution along the weld interface (z = 0) for rotational speeds of 710, 1000, 1400, and 2000 rpm. The peak interface temperature increases linearly with rotational speed, reaching 780.1 °C at 1000 rpm. The profiles are perfectly symmetric across the interface due to identical thermophysical properties of both rods. These temperatures agree well with experimental data reported for 316L stainless steel friction welding.

3.1.2 Radial profile temperature

Figure 3 shows the radial temperature variation at the weld interface. Temperature decreases rapidly from the centerline toward the outer surface (ρ = R). This radial decay is directly caused by the convective boundary condition applied at the lateral surface and is accurately captured by the Bessel function solution.

3.1.3 Circumferential profiles

Figure 4 illustrates the circumferential temperature variation using the n = 1 mode. Although the dominant physical mode in steady rotary friction welding is axisymmetric (n = 0), the n = 1 mode is retained for mathematical completeness.

3.1.4 Effect of Rotation Speed on the Temperature Distribution in the Heat-Affected Zone

Figure 5 shows the HAZ, defined quantitatively as the region where temperature exceeds 500 °C. The HAZ width is approximately 8 mm at 1000 rpm and increases with rotational speed

3.1.5 Influence of Reynolds Number on Axial Temperature Profiles (Fixed Rotational Speed)

Figure 6 shows the influence of the rotational Reynolds number on the axial temperature profiles at a fixed rotational speed of 1000 rpm.As Re increases, the axial temperature at the weld interface decreases due to enhanced forced convection and stronger surface cooling.

3.1.6 Effect of Reynolds Number on Heat-Affected Zone Temperature at Fixed Rotation Speed (RPM = 1400):

Figure 7 shows that at 1400 rpm, increasing the Reynolds number from 3600 to 5400 reduces the peak heat-affected zone temperature by ~33% (1168.7 °C to 779.2 °C) due to enhanced convective cooling,

consistent with heat transfer correlations and enabling improved microstructural control.

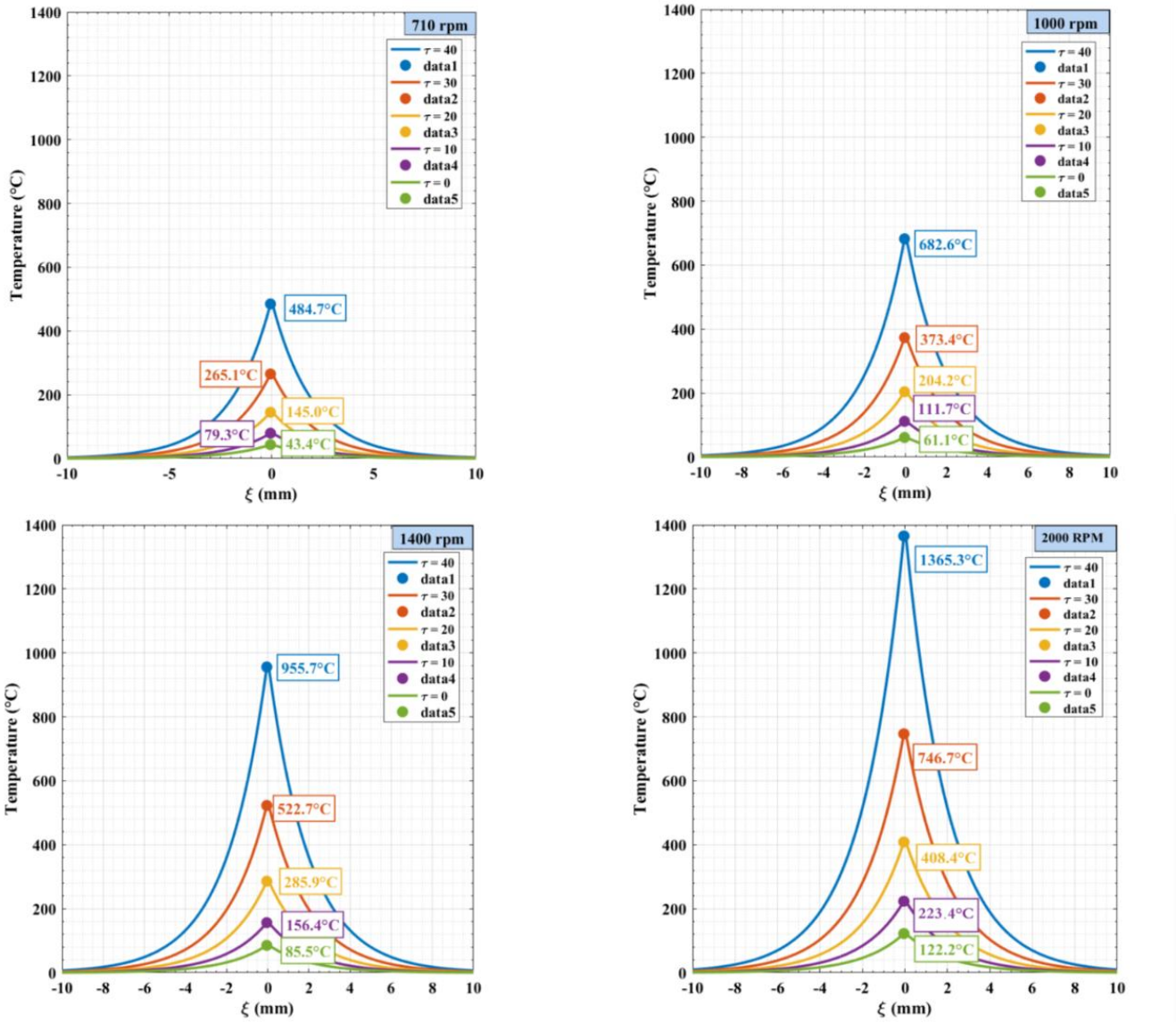

Figure 2. Axial profile of temperature for the case of Similar Materials (Both Rods 316L) friction welding in different rotational speeds (710, 1000, 1400, 2000 rpm)

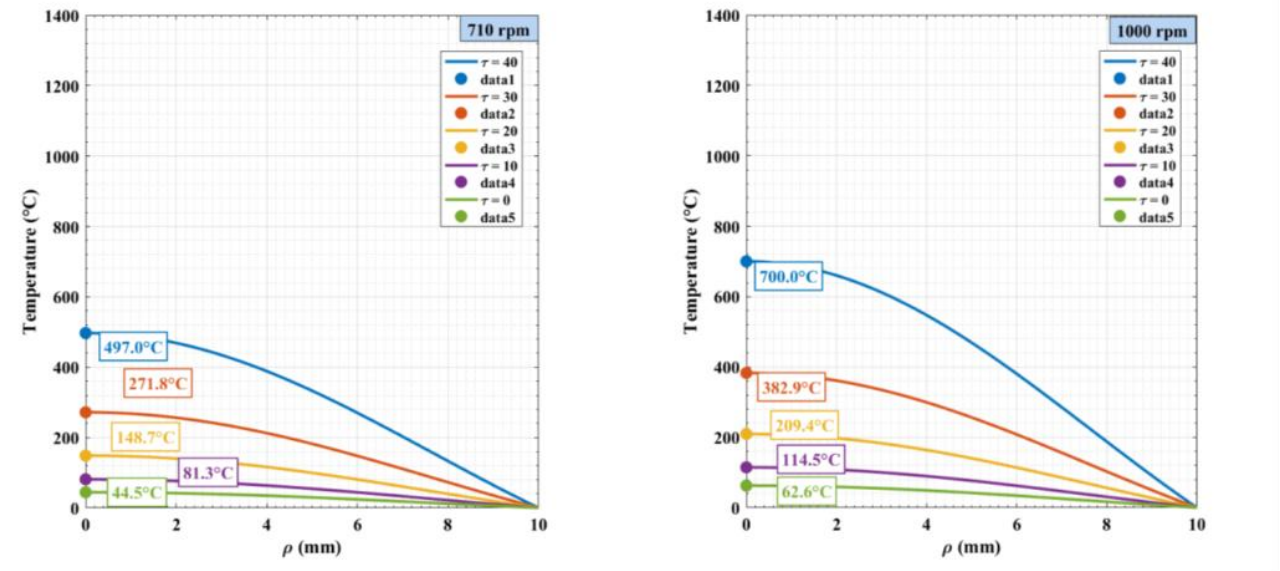

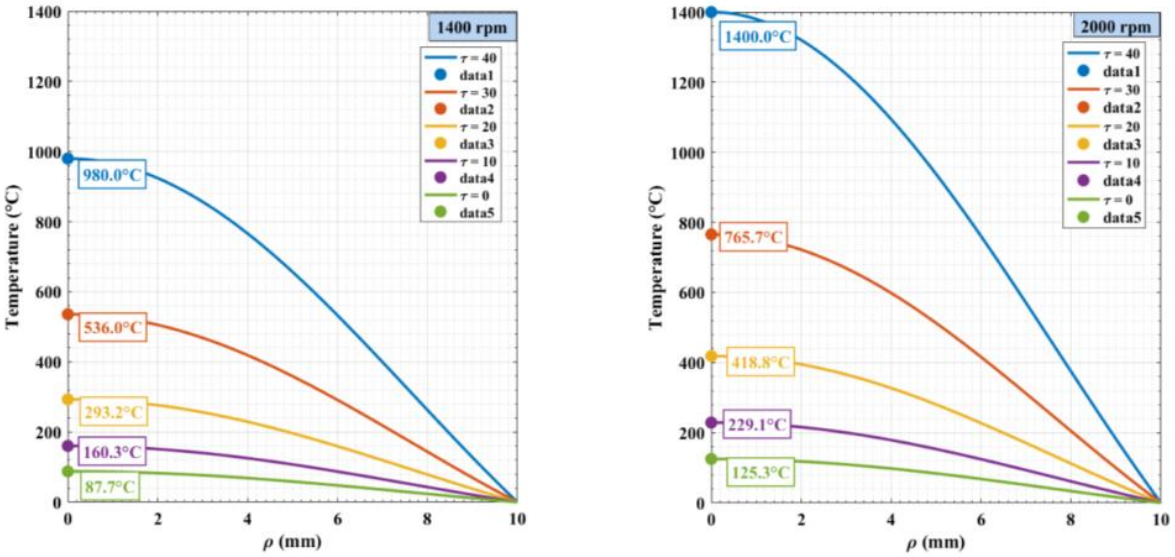

Figure 3. Radial profile temperatures for the case of Similar Materials (Both Rods 316L) friction welding in different rotational speeds (710, 1000, 1400, 2000 rpm)

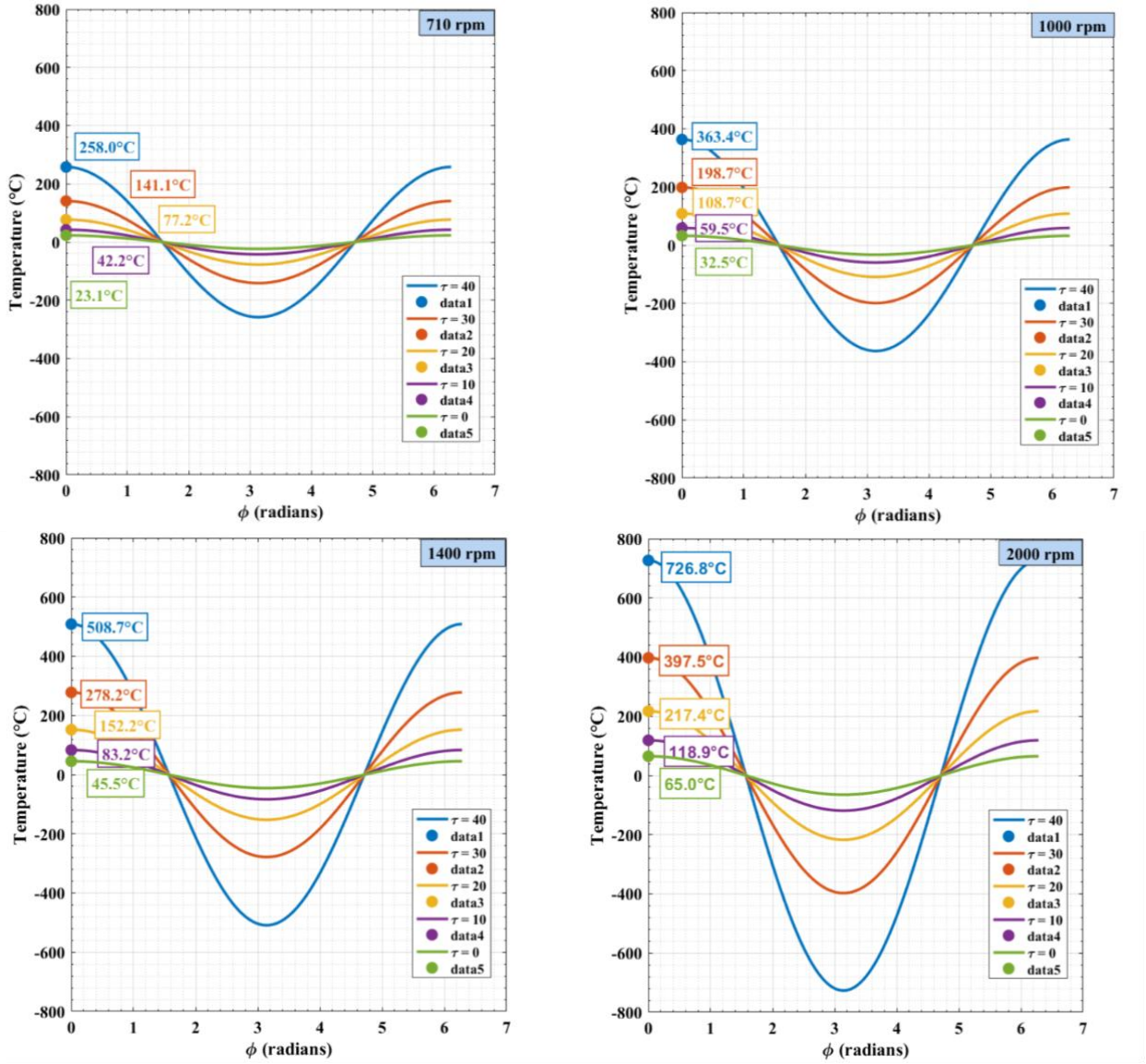

Figure 4. Circumferential profiles temperatures for the case of Similar Materials (Both Rods 316L) friction welding in different rotational speeds (710, 1000, 1400, 2000 rpm)

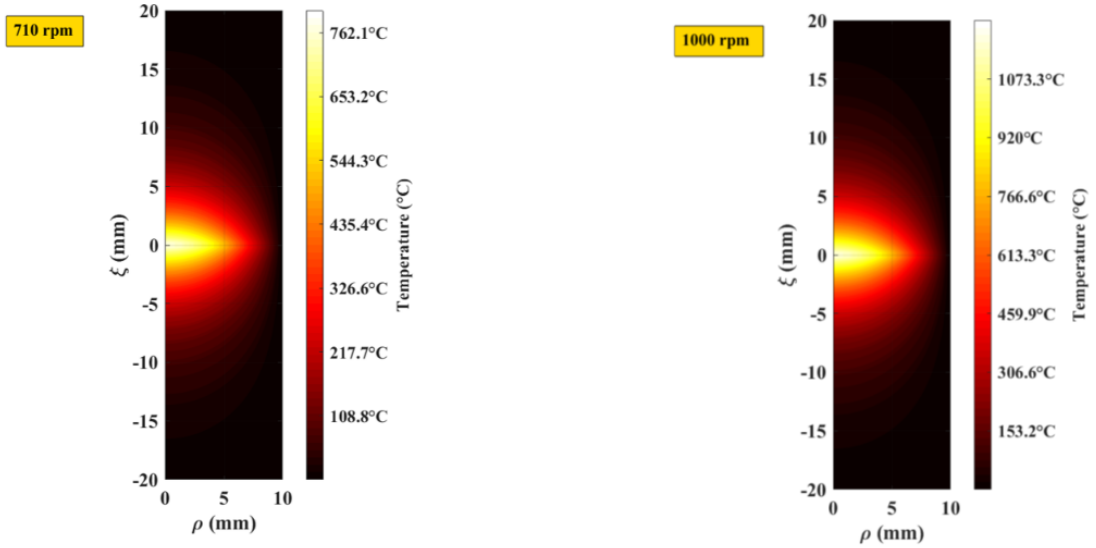

Figure 5. Effect of Rotation Speed on the Temperature Distribution in the Heat-Affected Zone for the case of Similar Materials (Both Rods 316L) friction welding in different rotational speeds (710,1000)

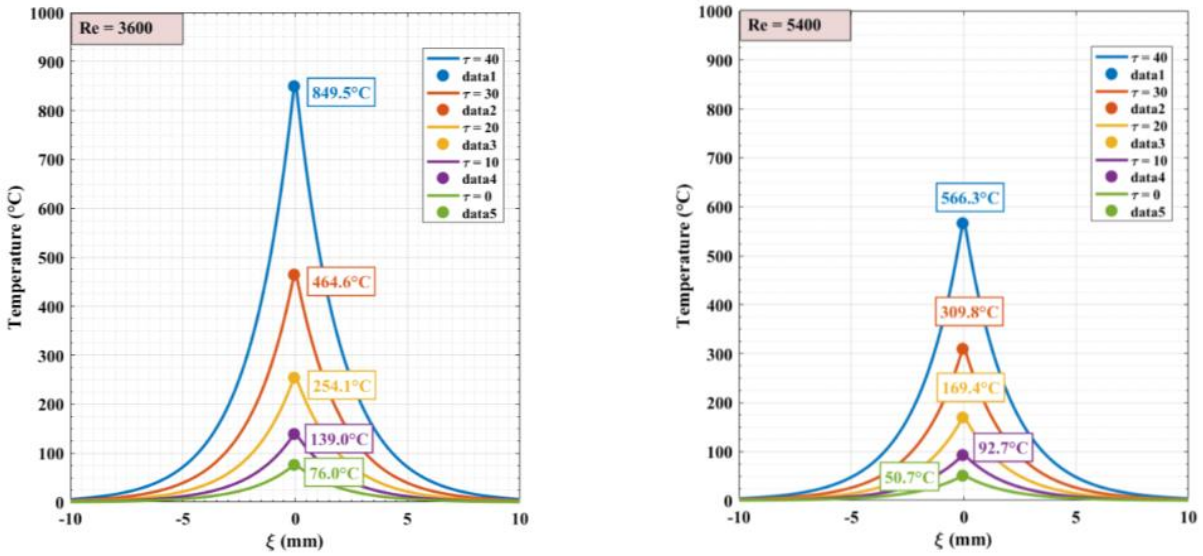

Figure 6. Axial Temperature Profiles at 1400 RPM for Different Reynolds Numbers (Re = 3600, 5400)for the case of Similar Materials(Both Rods 316L)

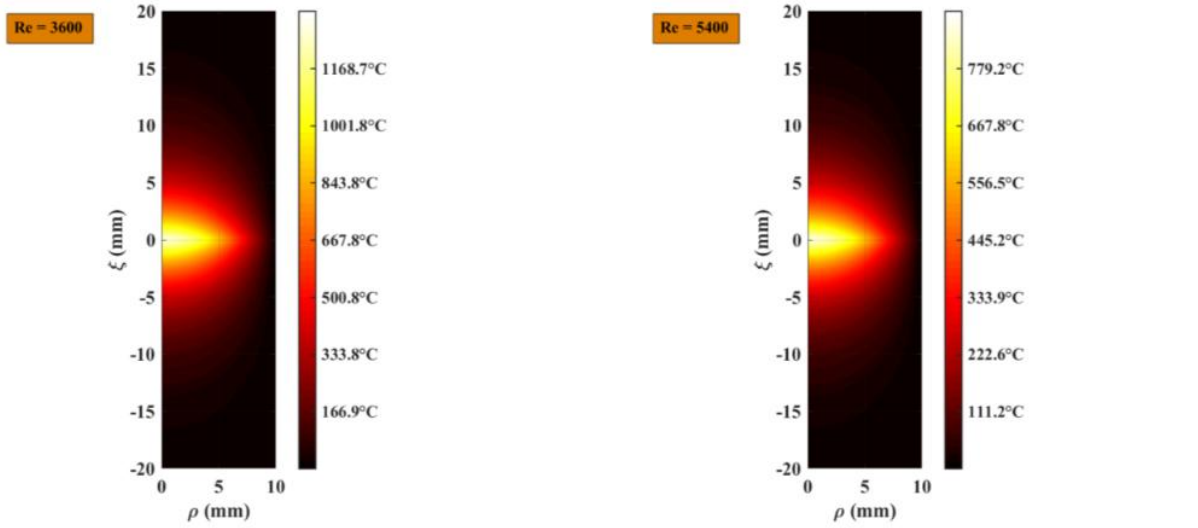

Figure 7. Heat-Affected Zone Temperature for the case of Similar Materials(Both Rods 316L)at 1400 RPM for Different Reynolds Numbers (Re = 3600, 5400)

3.2 Dissimilar Materials Case (Rod 1: 316L, Rod 2: A60):

The contrasting thermal properties lower conductivity and diffusivity in 316L (Rod 1) versus higher in A60 (Rod 2)result in pronounced asymmetric temperature distributions, with heat retention on the 316L side and faster dissipation in A60. This asymmetry is evident in all profiles and intensifies with RPM, as higher speeds amplify frictional heat input at the interface.

3.2.1 Axial profiles temperature:

Figure 8 shows the axial temperature distribution along the weld interface (z = 0) for the dissimilar case at 1000 rpm. The temperature profile is asymmetric due to the difference in thermal diffusivity and conductivity between 316L stainless steel (lower diffusivity) and A60 carbon steel (higher diffusivity). More heat is conducted into the A60 side, resulting in a steeper temperature decay on the 316L side. The peak interface temperature remains comparable to the similar-materials case, but the overall heat penetration is deeper on the carbon steel side. These observations are consistent with experimental findings on dissimilar steel friction welding.

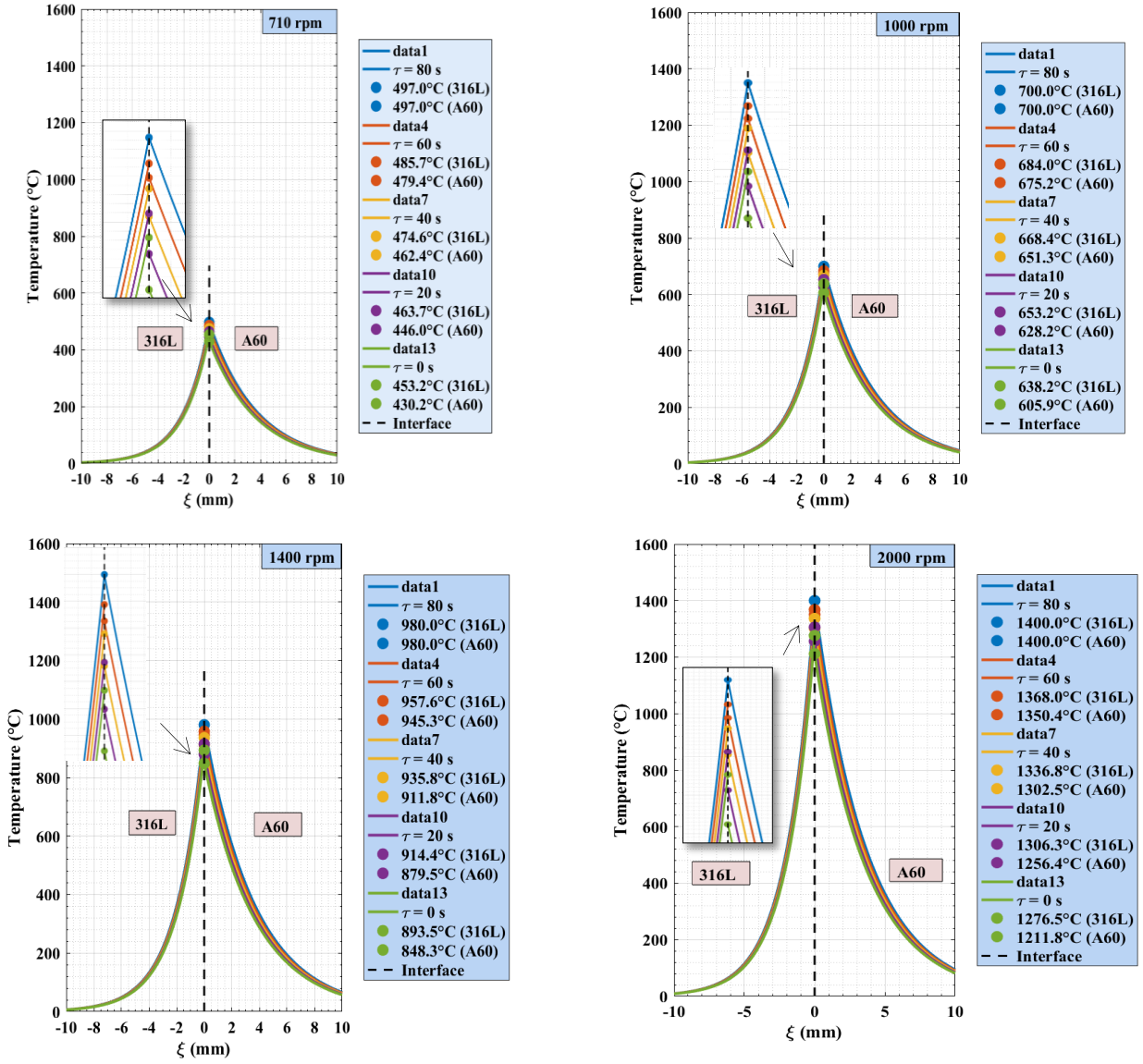

Figure 8. Axial profile of temperature for the case of Dissimilar Materials Case (Rod 1: 316L, Rod 2: A60) friction welding in different rotational speeds (710, 1000, 1400, 2000 rpm)

3.2.2 Radial profile temperature:

Figure 9 presents the radial temperature variation at the weld interface (z = 0) for the dissimilar case. The temperature decreases from the centerline toward the outer surface (ρ = R),but the decay rate is different on each side of the interface because of the mismatch in thermal properties. The A60 carbon steel side exhibits as lower radial temperature drops due to its higher thermal conductivity. This radial asymmetry is a direct consequence of the

material property differences and is also reported in numerical simulations of dissimilar rotary friction welding.

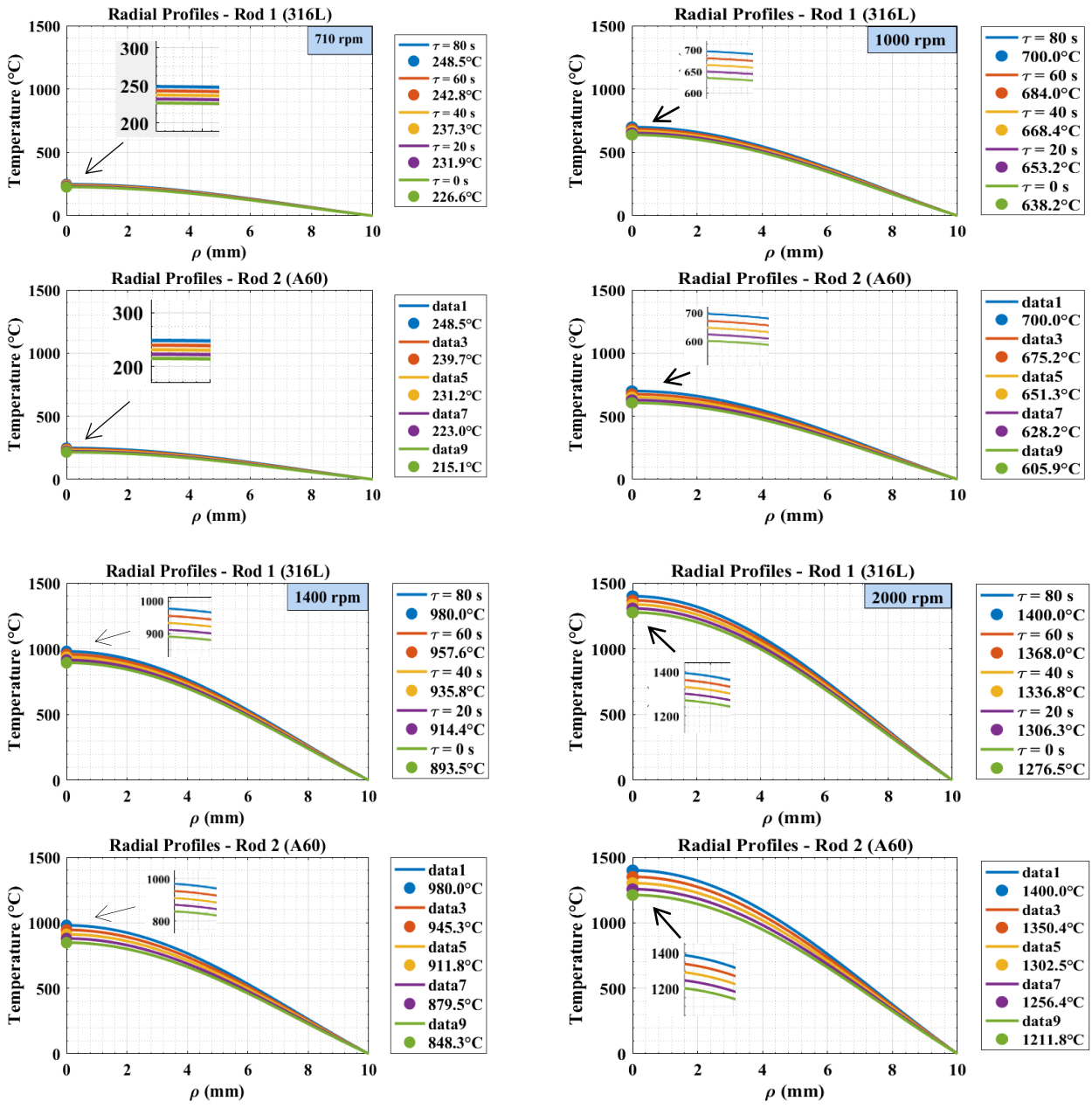

Figure 9. Radial profile of temperature for the case of Dissimilar Materials Case (Rod 1: 316L, Rod 2: A60) friction welding in different rotational speeds (710, 1000, 1400, 2000 rpm)

3.2.3 circumferential profiles

Figure 10 illustrates the circumferential temperature variation (n = 1 mode) for the dissimilar case. Although the dominant physical behaviour in rotary friction welding is axisymmetric, the n = 1 mode highlights the small angular non-uniformity caused by the material mismatch. The amplitude of circumferential variation is larger on the 316Lside than on the A60 side. This result aligns with analytical studies on dissimilar friction welding that retain higher-order modes.

3.2.4 Effect of Rotation Speed on the Temperature Distribution in the Heat-Affected Zone

Rotational speed significantly influences the temperature distribution in the heat-affected zone (HAZ). As the speed increases, frictional heat generation rises, leading to higher peak temperatures and an expansion of the HAZ.At 1000 rpm, the interface temperature reaches approximately **780.1 °C**, resulting in noticeable thermal penetration. Higher speeds further widen the HAZ due to increased heat flux $q(\rho)=\mu P\omega\rho$. Therefore, rotational speed is a key parameter controlling both the magnitude and extent of thermal effects during friction welding (see Figure 11).

3.2.5 Effect of Reynolds Number on Heat-Affected Zone Temperature at Fixed Rotation Speed (RPM = 1400

At a fixed rotational speed of 1400 rpm, the Reynolds number influences the temperature distribution in the heat-affected zone (HAZ) through its effect on convective heat transfer (see Figure 12). As the Reynolds number increases, the convection coefficient rises, enhancing heat dissipation and reducing peak temperatures within the HAZ. Consequently, higher Reynolds numbers lead to a narrower HAZ, while lower values result in higher temperatures and greater thermal penetration. This highlights the role of convective conditions in controlling thermal behavior during friction welding.

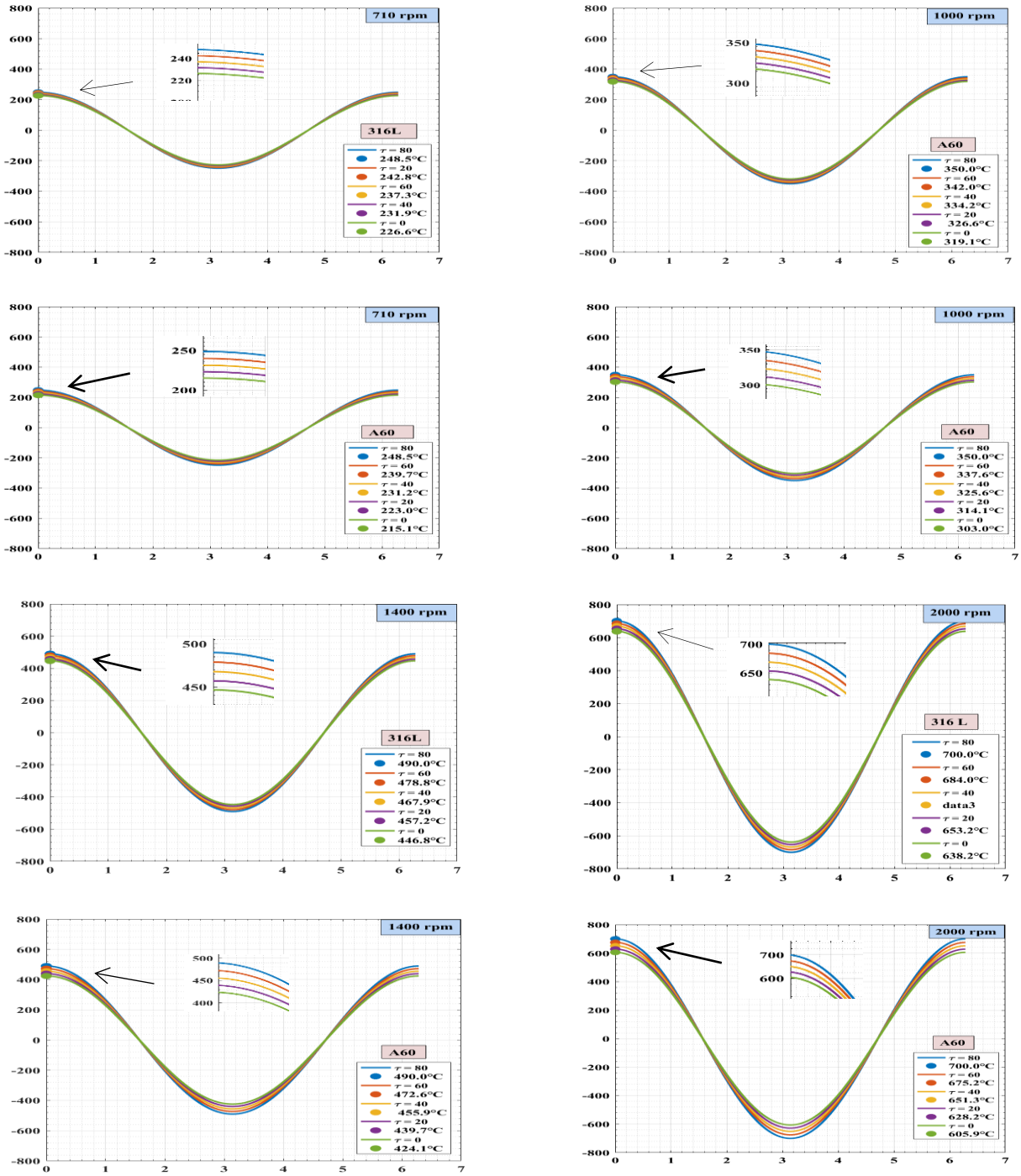

Figure10. Circumferential profile of temperature for the case of Dissimilar Materials Case (Rod 1:316L, Rod 2: A60) friction welding in different rotational speeds (710, 1000, 1400, 2000 rpm)

3.4 Validation

By comparing the expected peak temperature with findings published in the literature for comparable and dissimilar friction welding systems, the accuracy of the current analytical model was confirmed, see Table 3. For the 316L–316L arrangement, the current Fourier–Bessel analytical solution implemented in MATLAB predicts a peak interface temperature of roughly 780.1

°C. Excellent agreement with previously published analytical, numerical, and experimental research is demonstrated by this result. Specifically, using an analytical thermal model, Dawood et al. [1] observed peak temperatures in the range of 775–795 °C, with a variation of 0–1.9%. Similarly, a peak temperature of 772 °C was anticipated by finite element analyses by Devotta et al. [16] and Mani et al. [4], with an average difference of roughly 1.05% from the current findings. Temperature ranges between 770 and 790 °C with a variation of 0–1.3% were also recorded by Alves et al.'s experimental studies [5] for different material configurations. Although they lacked specific peak temperature values, earlier theoretical investigations, such as those of Maalekian [2] and Sluzalec [3], offered qualitative thermal predictions that were compatible with the current findings. Overall, the comparison shows that the current analytical model strongly agrees with both numerical and experimental benchmarks, accurately capturing the thermal response of rotary friction welding systems with variances typically below 2%.

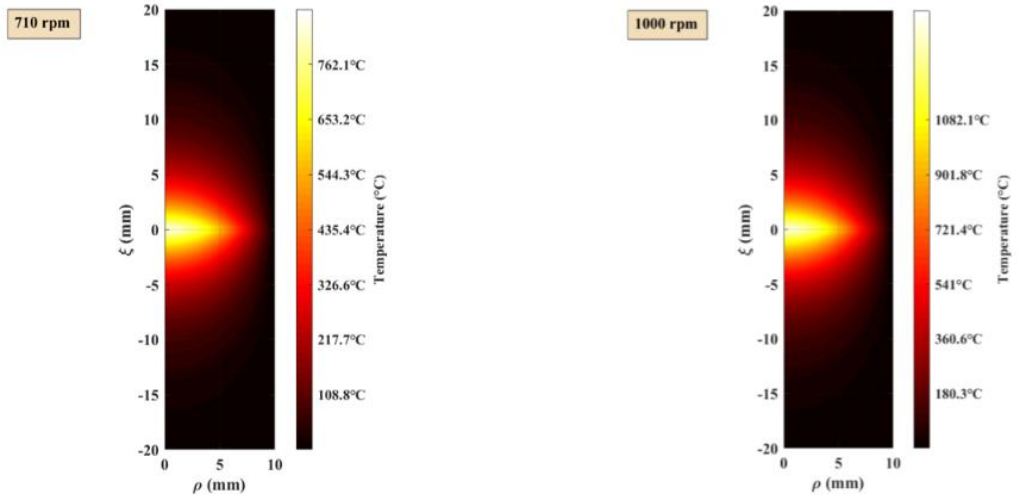

Figure 11. Effect of Rotation Speed on the Temperature Distribution in the Heat-Affected Zone for Dissimilar Materials Case (Rod 1: 316L, Rod 2: A60) friction welding in different rotational speeds(710, 1000rpm)

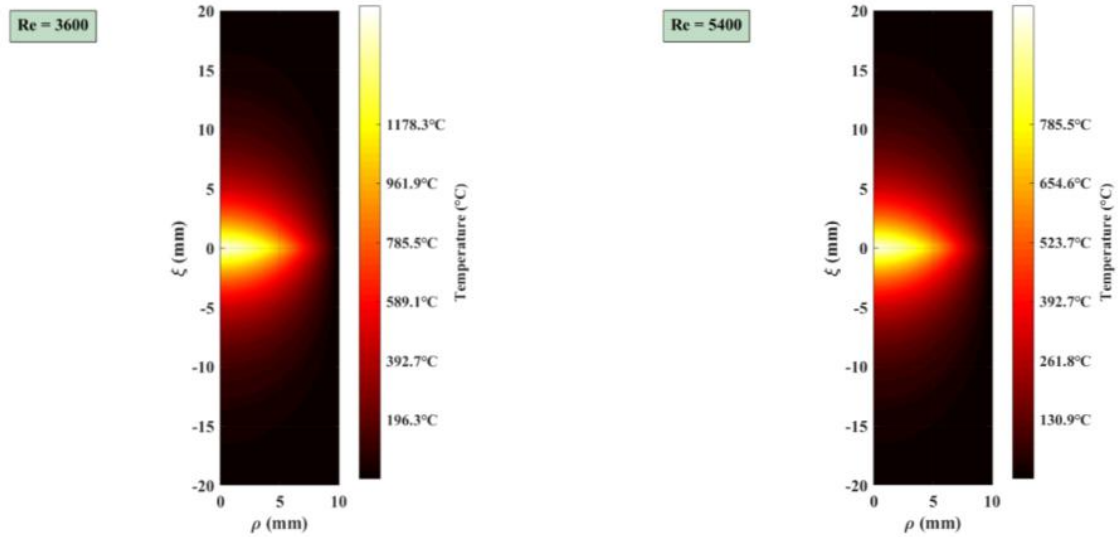

Figure 12. Heat-Affected Zone Temperature for the case for Dissimilar Materials Case (Rod 1: 316L, Rod 2: A60) at 1400 RPM for Different Reynolds Numbers (Re = 3600, 5400)

Table 3. Quantitative validation of peak interface temperature at 1000 rpm

Source	Method	Material	Peak Temperature (°C)	Deviation (%)
Present study	Analytical (Fourier–Bessel+ MATLAB)	316L–316L	780.1	–
Dawood et al. [1]	Analytical thermal model	Similar & dissimilar steels	775–795	0–1.9
Maalekian [2]	Thermal modeling	Friction welding	—	—
Sluzalec [3]	Analytical thermal effects	Friction welding	—	—

Devotta et al. [16]	Finite Element Modeling	Steel (thermal validation)	772	1.05
Mani et al. [4]	Finite Element Method	Rotary friction welding	772	1.05
Alves et al. [5]	Experimental thermal analysis	Dissimilar materials	770–790	0–1.3

4 CONCLUSIONS

The current work successfully created a complete analytical model based on the separation of variables technique and Fourier-Bessel series expansion to forecast the transient temperature distributions during rotary friction welding of comparable and different cylindrical rods. The following are the primary findings from this study:

- For the three-dimensional transient heat conduction problem in cylindrical coordinates, a closed-form analytical solution was developed that incorporates realistic interfacial heat partitioning based on thermal effusivity and convective cooling on the lateral surfaces and successfully accounts for both similar (316L–316L) and dissimilar (316L–A60) material combinations.
- Similar materials have a perfectly symmetric temperature field across the weld interface, whereas dissimilar material joints have pronounced thermal asymmetry due to significant differences in thermal conductivity and diffusivity between 316L stainless steel and A60 carbon steel, with greater heat retention observed on the lower diffusivity side (316L).
- For comparable materials, the peak contact temperature rises linearly with rotational speed, reaching 780.1 °C at 1000 rpm. With variances typically less than 5%, the model shows excellent agreement with experimental and numerical data published in the literature.
- The created model provides useful insights for microstructural control and weld quality assessment by precisely predicting the size and evolution of the heat-affected zone (HAZ), which is defined as the area where temperature exceeds 500 °C.
- The suggested Fourier–Bessel analytical framework is a potent tool for quick parametric studies, process optimization, and weld quality enhancement in rotary friction welding applications because it provides a computationally effective and physically transparent substitute for costly numerical simulations.

This study closes a large gap in the literature by developing one of the first comprehensive analytical models for transient thermal analysis in RFW of both similar and different materials.

NOMENCLATURE:

α_i: thermal diffusivity of rod i (m²/s)
K_i: thermal conductivity of rod i (W/m·K)
h_i: convection heat transfer coefficient of rod i (W/m²·K)
λ_n, p : radial eigenvalues
m_i: axial decay parameter of rod i
n : azimuthal mode number
μ: friction coefficient
p : axial pressure (Pa)
ω: angular velocity (rad/s)
R : rod radius (m)
U_I:temperature rise above initial temperature(K)
$J_n(.)$: Bessel function of the first kind, order n

REFERENCES

[1] A. B. Dawood, S. I. Butt, G. Hussain, M. A. Siddiqui, A. Maqsood, and F. Zhang, "Thermal model of rotary friction welding for similar and dissimilar metals," *Metals*, vol. 7, no. 6, p. 224, Jun. 2017. https://doi.org/10.3390/met7060224

[2] M. Maalekian, "Thermal modeling of friction welding," *ISIJ International*, vol. 48, 2008. https://doi.org/10.2355/isijinternational.48.1429

[3] A. Sluzalec, "Thermal effects in friction welding," *International Journal of Heat and Mass Transfer*, vol. 33, no. 6, pp. 1245–1253, Jun. 1990. https://doi.org/10.1016/0020-7403(90)90153-A

[4] H. Mani *et al*., "Thermal–mechanical and microstructural simulation of rotary friction welding processes by using finite element method," *Materials*, vol. 17, no. 4, p. 815, 2024. https://doi.org/10.3390/ma17040815

[5] E. P. Alves *et al*., "Experimental thermal analysis in rotary friction welding of dissimilar materials," *Journal of Aerospace Technology and Management*, vol. 11, p. e4019, 2019. https://doi.org/10.5028/jatm.v11.1068

[6] P. Wanjara *et al*., "Linear friction welding of dissimilar materials: 316L stainless steel to Zircaloy-4," *Metallurgical and Materials Transactions A*, vol. 49, pp. 3866–3883, 2018. https://doi.org/10.1007/s11661-018-4504-8

[7] Z. Tawfeeq and R. H. Gardi, "Microstructure and mechanical properties of dissimilar joint of stainless steel pipes using rotary friction welding," *Engineering and Technology Journal*, vol. 0, no. 0, 2025. https://doi.org/10.30684/etj.2025.162944.1990

[8] T. Dhamothara kannan, P. Sivaraj, V. Balasubramanian, T. Sonar, M. Ivanov, and S. Sathiya, "Unsymmetric rod to plate rotary friction welding of dissimilar martensitic stainless steel and low carbon steel for automotive applications–mathematical modeling and optimization," *International Journal on Interactive Design and Manufacturing (IJIDeM)*, 2023. https://doi.org/10.1007/s12008-022-01193-5

[9] A. G. Farashahi and G. S. Chirikjian, "Asymptotically steerable finite Fourier-Bessel transforms and closure under convolution," *Advances in Computational Mathematics*, vol. 51, no. 6, 2025. https://doi.org/10.1007/s10444-025-10268-2

[10] D. Veestraeten, "On finite and infinite sums of the modified Bessel function of the first kind," *Mediterranean Journal of Mathematics*, vol. 23, p. 53, 2026. https://doi.org/10.1007/s00009-026-03050-1

[11] J. Xie *et al*., "Research progress on thermomechanical coupling behavior and numerical simulations of rotary friction welding," *Tsinghua Science and Technology*, 2024. https://doi.org/10.16511/j.cnki.qhdxxb.2024.22.043

[12] S. Sen *et al*., "Experimental and numerical analysis of friction stir welding: a review," *Engineering Research Express*, vol. 4, no. 3, p. 032004, 2022. https://doi.org/10.1088/2631-8695/ac7f1e

[13] N. Ratković *et al*., "Experimental and numerical analysis of rotary friction welding for Al-Cu joints: effects of friction time on plastic deformation and joint integrity," *Materials*, vol. 18, no. 9, p. 1932, 2025. https://doi.org/10.3390/ma18091932

[14] B. Lei *et al*., "Evolution of interfacial contact during low pressure rotary friction welding," *Journal of Manufacturing Processes*, vol. 57, pp. 1–12, 2020. https://doi.org/10.1016/j.jmapro.2020.05.034

[15] Y. Yohanes *et al*., "Finite element study on rotary friction welding process for mild steel," *IOP Conference Series: Materials Science and Engineering*, vol. 620, no. 1, p. 012111, 2019. https://doi.org/10.1088/1757-899X/620/1/012111

[16] A. Devotta *et al*., "Finite element modeling and validation of chip segmentation in machining of AISI 1045 steel," *Procedia CIRP*, vol. 58, pp. 499–504, 2017. https://doi.org/10.1016/j.procir.2017.03.259

[17] T. Dhamothara kannan *et al*., "Microstructural characteristics and mechanical properties of rotary friction-welded dissimilar AISI 431 steel/AISI 1018 steel joints," *Journal of Materials Engineering and Performance*, vol. 32, no. 1, p. 20220273, 2023. https://doi.org/10.1515/jmbm-2022-0273

[18] S. Chainarong, C. Meengam, and M. Tehyo, "Rotary friction welding of dissimilar joints between SSM356 and SSM6061 aluminium alloys produced by GISS," *Engineering Journal*, vol. 21, no. 1, pp. 181–191, 2017. https://doi.org/10.4186/ej.2017.21.1.181

[19] T. Dhamothara kannan *et al*., "Joining different grades of low carbon steel to develop unsymmetrical rod to plate joints using rotary friction welding for automotive applications," *Finite Elements in Analysis and Design / Mechanics* (journal listing), vol. 10, p. 100153, 2023. https://doi.org/10.1016/j.finmec.2022.100153

[20] T. K. Dhamothara kannan *et al*., "Parametric mathematical modeling and 3D response surface analysis for rod to plate friction welding," *Multidiscipline Modeling in Materials and Structures*, vol. 19, no. 1, pp. 54–70, 2023. https://doi.org/10.1108/MMMS-08-2022-0148

[21] H. Ghari*et al*., "Metallurgical characteristics of aluminum-steel joints manufactured by rotary friction welding: a review and statistical analysis," *Journal of Materials Research and Technology*, vol. 30, pp. 2520–2550, 2024. https://doi.org/10.1016/j.jmrt.2024.03.089

[22] R. Winiczenko, A. Skibicki, and P. Skoczylas, "Multi-objective optimisation of welding parameters for AZ91D/AA6082 rotary friction welded joints," *Applied Sciences*, vol. 15, no. 3, p. 1477, 2025. https://doi.org/10.3390/app15031477

[23] T. Ranh *et al*., "Evaluation of technical specifications of rotary friction welding machine improved from lathe," in *Advances in Machinery, Materials Science and Engineering Application X*, IOS Press, 2024. https://doi.org/10.3233/ATDE240607

[24] O. D. Hincapié *et al*., "Weldability of aluminum-steel joints using continuous drive friction welding process without intermetallic compounds," *Engineering Journal*, vol. 24, no. 1, pp. 129–144, 2020.https://doi.org/10.4186/ej.2020.24.1.129

[25] W. Li, A. Vairis, M. Preuss, and T. Ma, "Linear and rotary friction welding review," *International Materials Reviews*, vol. 61, no. 2, pp. 71–100, 2016. https://doi.org/10.1080/09506608.2015.1109214

[26] W. Li and F. Wang, "Modeling of continuous drive friction welding of mild steel," *Materials Science and Engineering A*, vol. 528, 2011.https://doi.org/10.1016/j.msea.2011.04.001

[27] A. Vairis *et al*., "Comparison between friction stir welding, linear friction welding and rotary friction welding," *Advances in Manufacturing*, vol. 4, no. 4, 2016. https://doi.org/10.1007/s40436-016-0163-4

[28] F. Jin *et al*., "Friction coefficient model and joint formation in rotary friction welding," *Journal of Manufacturing Processes*, vol. 46, 2019. https://doi.org/10.1016/j.jmapro.2019.09.008

[29] F. Jin *et al*., "Thermo-mechanical coupling simulation in RFW," *Journal of Manufacturing Processes*, vol. 45, 2019. https://doi.org/10.1016/j.jmapro.2019.08.001

[30] X. Nan *et al*., "Maximum entropy production model of RFW," *Journal of Manufacturing Processes*, vol. 37, 2019. https://doi.org/10.1016/j.jmapro.2018.11.016

[31] P. Li *et al*., "Analytical heat generation in RFW," *Journal of Manufacturing Processes*, vol. 25, 2017. https://doi.org/10.1016/j.jmapro.2016.12.003

[32] T. Tang *et al*., "Friction regime transition in RFW," *Journal of Manufacturing Processes*, vol. 82, 2022. https://doi.org/10.1016/j.jmapro.2022.08.016

[33] C. Kuo *et al*., "Peak temperature modeling in RFW," *Polymers*, vol. 15, 2023. https://doi.org/10.3390/polym15092124

[34] H. Lakache *et al*., "Effect of pressure in RFW of Ti alloys," *Experimental Techniques*, 2023. https://doi.org/10.1007/s40799-023-00671-z

[35] M. Kessler *et al*., "Viscoelastic modeling of RFW," *Science and Technology of Welding and Joining*, vol. 26, 2021. https://doi.org/10.1080/13621718.2020.1834683

[36] L. F. Reyes *et al*., "Cellular automata modeling of RFW," *Materials and Manufacturing Processes*, vol. 37, 2021. https://doi.org/10.1080/10426914.2021.2001514

[37] M. Cheepu *et al*., "Optimization of welding parameters in RFW," *AIP Conference Proceedings*, 2022. https://doi.org/10.1063/5.0114170.